Donald T. Resio, Sea's the Future
Mark Loveland , USACE Engineering and Research Development Center

The Role of 4-Wave Interactions in Shoaling Water Depths

3rd International Workshop on
Wave, Storm Surges, and Coastal Hazards

1. Introduction

The objectives of this paper are 1) to synthesize the results from several recent studies that support a clear basis for a specific kinematic breaking criterion related to the ratio of the energy propagation velocity (i.e. group velocity) to the currents generated by longer waves; 2) to develop a methodology to quantify the rate and spectral distribution of energy loss due to wave breaking; and 3) to show a consistency between the predicted loss rate and the nonlinear fluxes into the portion of the spectrum dominated by breaking. Following a brief review of dynamic and kinematic bases for wave breaking, this paper will devote one section to each of the three objectives noted above. Our discussion will examine the potential role of the breaking formulation introduced here to the development of a transition from an f^{-4} to an f^{-5} form in the higher-frequencies of wave spectra.

Governing processes for spectral forms of wave breaking have been the subject of many prior publications and many different parameterized source terms for wave breaking in wave spectra propagating to a coast have been hypothesized, developed and implemented in coastal wave models. Although many authors have been somewhat emphatic that the energy fluxes due to wave-wave interactions governing wave breaking and dissipation is expected to be governed by Boussinesq equations, Onorato et al. (2007) showed that, provided conditions for convergence of wave expansion were met, four-wave interactions also provide an equivalent approximation for wave-wave interactions in waves propagating into shallow water. This paper builds upon the work of Ardag and Resio (2020), assuming that high-frequency wave breaking can be related to a kinematic breaking criterion can be included into wave models. In this context, the spectral shape will exist only when the source-term balance is dominated by four-wave interactions. Examples of spectra from storms at a buoy located offshore in a depth of about 18 meters and a linear array located in a depth of about 8 meters off the coast from the U.S. Army Corps of Engineers Field Research Facility are shown in Figure 1.

Figure 1 shows that the shape of these spectra normalized by wave number, i.e.

$$1. \quad \overline{F}(\hat{k}) = \alpha_4 \left(\frac{k}{k_p} \right)^{-5/2}$$

can be represented by equation 1, where the overbar denotes a nondimensional quantity, k is the modulus of the wavenumber and k_p is the modulus of the wavenumber of the spectral peak In this figure a change in the normalized slope is observed This will be the key to our discussion of wave breaking in a spectral context in this paper.

Wave breaking, represented in spectral models as S_{brk}, is a critical process at the ocean-atmosphere interface that enhances gas exchange with air and water and transfers mass and momentum fluxes into the water column through the generation of turbulence (Melville, 1996). In a physical sense, S_{brk} is the least understood term among the source terms; it is temporally and spatially sporadic in the time domain and occurs on a much shorter time scale than other major source terms contributing to wave generation and decay (nonlinear resonant interactions and wind input). Hence, despite numerous scientific investigations over the years, S_{brk} has no universally accepted mathematical form (Holthuijsen, 2007). The complex and highly nonlinear character of wave breaking in random seas makes it very challenging to interpret S_{brk} on a time and space scale commensurate with the other source terms used in spectral wave models.

The interpretation of present instrument-based observations of energy dissipation in wind waves must be supported by visual observations to develop concepts for source terms (Babanin et al., 2001; Banner et al., 2000; Romero et al., 2012; Schwendeman et al., 2014). Even in this context, it is only possible to locate these events in space but it is not straightforward to estimate the spectral distribution of associated energy losses in frequency and wave propagation angle.

Dynamic, kinematic and geometrical criteria have all been employed to characterize limits for an incipient wave breaking mechanism and to determine the onset of breaking. The most commonly used criteria in spectral wave models today, wave steepness. Wave steepness in monochromatic, unidirectional waves of permanent form has been well studied (Gerstner, 1809; Stokes, 1880); and a theoretical basis for extending the steepness concept to spectra can be found in Alves & Banner (2003) and within the context of narrow-banded in frequency by Song & Banner (2002). Experimental evidence supporting the theoretical developments are given in Banner & Peirson (2007). Other attempts to extend the concept of steepness-limited breaking have been founded on dimensional arguments which suggest that spectral steepness in directionally integrated spectra typically are consistent with an f^{-5} form, i.e. $E(f) \propto \alpha g^2 f^{-5}$, where f is frequency, g is gravity and α is a dimensionless constant originally presumed to be a universal constant Phillips (1958)). More recently, the equilibrium range has been based on the premise that a balance between wind entering this range from the near-peak region and the development of a constant flux rate by nonlinear interactions leads to an equilibrium shape in deep water with an f^{-4} form, for example, Zakharov and Filenenko (1967), Toba (1973), Donelan et al. (1998), Resio and Perrie (1989).

The approach followed here will provide evidence that breaking that is limited primarily to the high frequency portion of the spectrum. Given that wave breaking occurs sporadically in time and space on the wave surface it is unlikely that wave breaking can be well represented by a process occurring in a purely spectral domain; instead, when a wave breaks all frequencies within the area encapsulated by the 4-dimensional space-time volume in which breaking occurs is energy is lost. In this context, wave breaking becomes a function of local conditions that exceed a common breaking threshold distributed in space and time on the sea surface. Solving for these exceedances must be performed in time and space as discrete breaking events, rather than as a continuous spectral dissipation function. In turn, this is expected to produce a variation in the spectral shape at the frequency where this transition occurs, since the spectral form above this threshold is expected to be dominated only by gravity and frequency as postulated by Phillips, 1958, suggesting that the spectral form in this spectral region should follow an $E(f) \propto g^2 f^{-5}$ form, Most observations today support an equilibrium range is dominated by a $\beta g f^{-4}$ where β is an empirical constant with units of velocity (Toba 1972; Donelan et al. 1986, Resio et al. 2004). Recent studies have shown that in many if not most situations spectra contains both spectral forms with the f^{-5} always located at higher frequencies that the f^{-4} range (Romero. Et al, 2012, Resio and Ardag (2016), Ardag and Resio (2019).

Recent numerical, laboratory, and field data have shown that wave breaking appears to be linked to a specific kinematic threshold. Such a threshold is developed as a function of wave celerity to the ratio of the current velocity at the water surface. A new breaking source term (Ardag and Resio, 2020) has been shown to be consistent with kinematic limits for incipient, sporadic wave breaking within a statistical framework for the occurrence of threshold exceedances. A critical assumption adopted here is that, although wave breaking is recognized to be related to wind speed, as noted by many empirical relationships proposed between wind speed and percentage white cap coverage, it should be derived independently from the wind input term to enable its ability to represent variations in breaking as a function of wave age, shallow-water effects, and other nonlinear processes.

Previous Research on Wave Breaking

Literature dedicated to wave breaking has extensively examined two questions relevant to nearshore wave modeling: 1) What physical process leads to wave breaking? (Breaking onset in individual waves) and, 2) What role does wave breaking play in the evolution of wave spectra, within the spectral dissipation source term? Finding an answer to the first question does not provide a straightforward means to specify the spectral consequences of breaking for the latter of these questions. Since sporadic breaking is observed in wind seas at a range of scales. An additional step is required for application of monochromatic concepts to phase-averaged wave modeling. In this paper, we address these two research problems within a single coherent framework, starting here with wave breaking.

Considerable research has improved our understanding of the wave breaking process in wind waves. For example, Rapp and Melville (1990) and Tulin and Landrini, 2001 showed that breaking could occur at low steepness values, *ak*, in the range of 0.15 to 0.2. Toffoli et al. (2010) combined deep water observations and laboratory measurements to show waves could exist past this steepness limit even though they fall only partially within the breaking phase of such waves. The kinematic criterion for wave breaking relates horizontal velocities at the water surface (typically occurring at or near the crests of large waves) to the group or phase velocity of a waves that are temporally and spatially coincident with these larger waves. This framework limits the particle velocity at the tip of a wave crest to some fraction of the wave propagation speed.

A much more complete review of the research of wave breaking can be found in Ardag and Resio (2020) and will not be repeated here. An overview of this developments follows. A compilation of research into wave breaking led Banner and Tian (1998) to suggest that the ratio of the particle velocity ant the surface to the group velocity U/C_g should be limited by a universal value estimated to be about 0.8. The main conclusion drawn by Irisov & Voronovich, (2011) was that the dominant breaking in random wave fields occurs at intermediate frequencies rather than at the spectral peak or only at very high frequencies. This concept was superseded by a unique study by Waseda et al. (2014) in which they recorded characteristics of the deep ocean surface waves, including extreme waves, by deploying a moored buoy and a drifting buoy. The GPS sensors on these buoys allowed them to measure horizontal displacements on the wave surface and estimate orbital velocities which provided a Lagrangian framework as opposed to the more conventional Eulerian observational basis for analysis. When waves move to the peak of the group, speed of the particles at the crest accelerates, even if they are not breaking (Tulin and Landrini, 2001). Looking at the U/C_g (normalized maximum horizontal particle speed) values from their deep water observations, Waseda et al. (2014) were able to show that there is a threshold (0.85-0.9) after almost all waves at higher frequencies break. Another interesting point from their work was that their ensemble of observed spectra in deep water followed an f^{-4} form in the equilibrium range. The implication here is that even during low wind and/or low steepness (low breaking) conditions nonlinear interactions are able to keep the spectra in this form in spite of active wave breaking.

A substantial body of evidence now exists supporting the existence of an equilibrium range located just above the spectral-peak region. The characteristic $k^{-2.5}$ spectral form in shallow areas (consistent with an f^{-4} in deep water) is consistent with both field measurements and theoretical perspectives (refs). This kinematic criteria appears to provide a robust representation of wave breaking, and we shall utilize this approach in our transition to a dissipation source term for wave spectra at high frequency into a spectral range later in this paper. There seems to be some disparity in the literature when it comes to the use of phase speed or the group speed as the basis for the ratio shown above, depending on the numerical experiment, laboratory or even field measurements. For this reason, we chose to make our decision be consistent with our own modeling framework. This scale perspective suggests that since refraction and diffraction effects occur on a scale smaller than a wavelength they should be related to phase velocity; whereas processes involving generation, convergence, and divergence of energy fluxes are associated with an averaging over the entire wave cycle and should be characterized by the group velocity. Therefore, in a spectral context, group velocity, which controls energy fluxes within spectrum is chosen here for the wave speed in our criterion for the likelihood of random wave breaking in a wave field.Steepness limits have been a fundamental basis for the dissipation source term in many operational wave models, possibly due to the convenience of applying it to wave spectra (Alves and Banner, 2003; Babanin et al., 2010; Komen et al., 1984). Alternative representations for this process include weak-in-the-mean forms (Hasselmann, 1974) in which breaking is linearly related to the wave number spectrum, prescriptive methods that lize a saturation limit (Alves and Banner, 2003; Phillips, 1985) and exceedance probability formulations for various wave quantities.

Ardag and Resio (2020) quantified the breaking characteristics of incipient breaking, based on kinematic criterion using simulated time series of surface water level, velocity at the surface and other characteristics at a fixed point for a range of sea states. In these simulations, wave records were generated at a single point by first assigning random phases on frequency components of f^{-4} spectra (i.e. without dissipation ranges and similar spectral structure to Resio et al., (2011), corresponding to different wind speeds and peak frequencies and then superposing each of them linearly ($N_{frq} = 191$) linearly spaced frequency increments between 0.05 and 1 Hz). A simple $\cos^4$ distribution for the angular spreading in the initial spectra. This analysis was repeated for a wide range of wave age values from young seas to mature swell.

Given the finite number of random frequency components, this is valid only for a given interval amount of time; however, variations in time simulated and seed values for the specification of the random phases produced only small variations in the number of wave-breaking events based on exceedance of the kinematic criterion. Using this approach, 200-second simulations were repeated within a Monte Carlo simulation to create long sets of random waves using 50 sets of 50 random numbers to generate 50 random 10000 second wave records for each sea state.

The height of the water surface at any time step is calculated from the linearizedapproximation,

2, 2

where z_{ifrq} is the individual contribution to the total surface height by each frequency component at a single point location in space and i_{frq} is the frequency increment. For unidirectional simulations z_{ifrq} is defined as,

$$3.\ z_{ifrq} = a_{ifrq}\cos(-\omega_{ifrq}t + \phi_{ifrq})$$

ϕ is the phase of the linear waves that is assigned at each discrete frequency and varies randomly between [0, π], *a* is the amplitude of the wave at each frequency constituent. An example of a 50 seconds surface record from Ardag an Resio is shown in Figure 2 which was created by using a wave spectrum corresponding to 4 second waves and 15 m/s wind speed. A zero-up crossing method was used to identify individual waves within the overall wave time series in these records which are marked in red circles in the figure.

Equation 2 contains enough components to reflect a random sea surface, however we initate our simulations with directional spectra. Including directional constituents into z_{ifrq} to run directional simulations produce the following form t in,

$$4.\quad \begin{aligned} z_{(ifrq,jdir)} &= a_{ifrq}\cos(k_{ifrq}x - \omega_{ifrq}t + \phi_{(ifrq,jdir)}) \\ z_{ifrq} &= \sum_{jdir=1}^{N_{dir}} z_{(ifrq,jdir)} \end{aligned}$$

The difference from the unidirectional form is that the phase depends on both frequency and angular components of the spectra. For our runs we considered 15 angle bands centered on the mean angle with 10 degree increments which covers a total of 150 degrees. For deep water k_{ifrq} is simply found by using the dispersion relationship $\omega_{ifrq}^2 = gk_{ifrq}$ where g is the gravitational acceleration. Considering both directional (15) and frequency(191) constituents, for every time step there are a total of about 2800 constituents included in these directional simulations.

In deep water, the horizontal orbital velocity U_{orb} of very small spectral components is $a_{ifrq}\omega_{ifrq}$, and, neglecting nonlinear interactions, for our unidirectional simulations has the form,

$$5.\ U_{orb}(i_{frq},t) = \int_{\omega_0}^{\omega_{ifrq}} a(i_{frq})\omega(i_{frq})\cos(-\omega t + \phi(i_{frq}))d\omega .$$

where $U_{orb}(i_{frq},t)$ is the estimated total orbital velocity at each frequency/time. At each time step, for every frequency constituent the integration limit increases from ω_0 to t. s. For directional tests, the form changes into the linearized summation represented by :

$$6.\ U_{orb}(i_{frq},t) = \int_{\omega_0}^{\omega_{ifrq}} \int_{\theta_{\min}}^{\theta_{\max}} a(i_{frq})\omega(i_{frq})\cos(k_{ifrq}x - \omega t + \phi(i_{frq}, j_\theta))d\omega d\theta$$

The where maximum orbital velocity for each up-crossing wave, was calculated as a function of the upper limit of the integrated term in equation 4. Using this approach, we only used a zero-up crossing method to define individual waves and found the associated maximum orbital velocities for these waves. This maximum value was then used to find the ratio, $max\left[U_{orb}(i_{frq},t)\right]/C_g(f)$ as a function of frequency where $C_g = g/2\omega$ within the up-crossing wave interval. Rearranging these terms, the frequency at which the ratio exceeds the kinematic limit, f_{brk} for each individual up-crossing wave is determined to be:

$$7.\ f_{brk} = \psi \frac{g}{(4\pi U_{orb})},$$

where ψ is the empirical coefficient established by the kinematic breaking criterion. Additional detail on this approach can be found in Ardag and Resio (2020)

2. Quantifying the role off nonlinear energy fluxes through the spectrum relative to energy losses from wave spectra

Assuming that breaking does not affect the spectrum at frequencies lower than the defined breaking frequency, the rate of dissipative energy loss must balance the nonlinear energy fluxes to high frequencies through the equilibrium range of the spectrum. Observational evidence (Lenain and Melville, 2017; Long and Resio, 2007; Romero and Melville, 2010) implies an inverse relationship between the wave age and the location of the transition zone. The rate of nonlinear energy fluxes to high frequencies depends on the energy level within the equilibrium range, which can be estimated by,

8. $\Gamma_B = \dfrac{\lambda \beta^3}{g}$, where β has the dimensions of velocity

and, since is represents a wave-wind interaction quantity, several different forms for it have been proposed.

have been and λ is a near-constant coefficient weakly related to angular spreading within the equilibrium region within a range of about 3-5. (Resio et al., 2001). Given the type of angular distributions chosen in our work, we used 5 in our experimental simulations.

The energy transferred into the breaking region by nonlinear fluxes should be lost in an average sense by the dissipation within the breaking zone. Our assumption is that the positive energy fluxes moving from spectral peak region towards high frequencies start to dissipate at the location of the transition from the f^{-4} form to an f^{-5} spectral form. The amount of energy lost t (E_b) in an individual wave that breaks, is approximated by,

Commented [A1]: Should we say individual wave or wave group here? Reviewers are pointing this out.

$$9.\ E_b = \int_{f_{brk}}^{\infty} \alpha_5 g^2 f^{-5} df = \frac{\alpha_5 g^2 f_{brk}^{-4}}{4} ,$$

where α_5 is a dimensionless coefficient analogous to the Phillips coefficient, evaluated at the breaking frequency. However, this coefficient must be evaluated at a point where the directionally integrated f^{-4} and f^{-5} spectra have the same value at this point, i.e.

10. $E(f_{brk}) = \beta g f_{brk}^{-4} = \alpha_5 g^2 f_{brk}^{-5}$. The frequency at which these two terms are found to match is termed the transition frequency, since the is the location at which the spectrum changes its form. Combining (6) and (8) we obtain the relationship. In this form, α_5 is dimensionless and we have at the transition frequency

11. $$\frac{\lambda\beta^3}{g} = \frac{\alpha_5}{4} g^2 f_{brk}^{-3}.$$

Combining equation (9) with equation (8) yields

12. $$\lambda\beta^2 = \frac{\alpha_4}{4} g^2 f_{brk}^{-2}.$$

Grouping constants and simplifying again:

13. $$\chi\beta = \frac{g}{f_{brk}}.$$

where χ is a coefficient that represents dimensionless constants derived from observations combined with the assumed value for the flux constant.

Resio et al. (2004) presented observational evidence that $\beta \approx (U_{10}{}^2 C_p)^{1/3}$, which when combined with $C_p = g/\omega_p$ and equation 11 we obtain the relationship:

14. $$\chi \frac{f_{brk}}{f_p} = \left(\frac{C_p}{U_{10}}\right)^{2/3}.$$

Consistent with observations, this relationship implies a relationship between inverse wave age and the breaking location where χ is a dimensionless coefficient that shifts location of the transition point with respect to the location of the spectral peak. We find it using nonlinear positive energy fluxes as will be explained in next section.

Over the total duration of the simulations for various initial spectra, breaking may occur at a large range of frequencies, as shown in Figure 3. However, the rate of energy loss is expected to depend on the recurrence of breaking and the amount dissipated energy of a particular frequency constituent. For lower transition frequencies, the nonlinear energy loss rate relative to breaking is high, indicating that the magnitude of positive energy fluxes into is large the breaking range is high. The loss rate is somewhat analogous to a turbulence cascade in with the total energy loss rate given by,

$$15.\ \left(\frac{\partial E_b}{\partial t}\right)_i = \frac{\sum_{f_i}^{f_i+\Delta f} E_b}{T_{tot}}\ \text{, where, } \left(\frac{\partial E_b}{\partial t}\right)_{f_{ti}} \square \left(\Gamma_B\right)_{f_{ti}},$$

where T_{tot} is the total run time. This produces a Phillips f^{-5} spectral form in which sporadic breaking maintains an energy cascade, similar to that found in other turbulent cascades. A major difference from the initial breaking assumption by Phillips that the empirical coefficient (α_5

in equation 7) is a constant, while the value of this coefficient in our formulation must vary with to match the value of the equilibrium range f^{-4} spectral form at the transition point f_{t_i}. Our simulations are executed for 500 000 seconds in unidirectional tests and 250 000 seconds in the directional tests. The frequency increment, Δf, is chosen to be 0.05 Hz, *i* is the frequency counter in these simulations, and f_{ti} is the transition frequency. Figure 4 shows the location of the nondimension "transition" frequency from these simulations as a function of inverse wave age taken from Ardag and Resio (2020).

Figure 5 is a representation for a single peak frequency and wind speed condition. To cover a wider range of the sea states, 24 different conditions from very young waves to well-developed waves were generated using peak frequencies of 0.15, 0.2, 0.25 and 0.3 Hz and wind speeds of 5, 10, 15, 20, 25 and 30 m/s. These simulations were initiated with 50 sets of 50 random seed values over a total duration of 500,000 seconds. The intersection points between the positive energy fluxes and the energy loss rates were found using the same methodology as introduced here for each case. To investigate the influence of the empirical coefficient of the kinematic criterion in equation (5) these tests were repeated for ψ values of 0.7, 0.8 and 0.9, yielding a total sample size with 72 points. Subsequently, these points were plotted against the estimate rates as a function of $(C_p/U_{10})^{2/3}$ to obtain Figure 5. This figure also contains linear fits for each of the empirical coefficients and their R^2 values.

As shown in Figure 6, the agreement between the two rates and the associated linear correlation values (R^2) is high for a range of inverse wave age. An examination of this plot shows that the value of for young waves the dissipation zone reaches to the peak; and the equilibrium range is essentially non-existent under these circumstances. On the other hand, when the wind speed is low the transition frequency (f_{ti}) shifts towards higher frequencies. For χ equal to 0.8, the linear relationship is given as,

$$16. \quad f_{ti} = \frac{f_{brk}}{f_p} = 1.4\left(\frac{C_p}{U_{10}}\right)^{2/3} + 0.54$$

We then compared results from unidirectional and directional tests for varying wave ages. Here, we initiated directional runs with ψ rate of 0.8 over a total duration of 250 000 seconds, completed the same analysis as explained above, and on Figure 7, we compared locations of transition frequencies for a wide range of sea states. As it is apparent from the figure, for all of these wind-sea conditions the difference is relatively small; thus, the initial assumption of unidirectional spectra can be considered to be a reasonable first approximation to directionally spread spectra.

These figures support the linear relationship given in equation (15) between the two parameters. In a modeling sense this relationship between wave age and the spectral form transition point could be used to define upper frequency of the f^{-5} tail. A comparison of this hypothesized relationship to field data by Long & Resio, (2007) was shown in Figure 1, where the compensated and normalized energy spectra were grouped by their inverse wave ages to indicate transition frequencies with black dots. Since the range of young waves (1.6 - 3.4) is bigger than the rest, in our comparisons the biggest inverse wave age considered was 1.6. Overall, comparison between the Figures 7 and 1 show good agreement between observed and predicted transition frequencies and Table 1 gives the relationship between the transition frequencies and the inverse wave age using results from the simulations.

3. Energy Fluxes into the wave breaking zone in shallow water

The governing processes for spectral forms of wave breaking have been the subject of many prior publications and many different parameterized source terms for wave breaking in wave spectra propagating to a coast have been hypothesized, developed and implemented in coastal wave models. Although many authors have been somewhat emphatic that the primary wave-wave interactions governing wave breaking and dissipation is expected to be governed by Boussinesq equations, Onorato et al. (2007) showed that, provided conditions for convergence of the 4-wave expansion were met, four-wave interactions could also provide a good approximation for waves in intermediate and shallow water as long as the expansion use in the derivation remained accurate.

In intermediate and shallow water, it is advantageous to simulate wave in wavenumber space rather than in frequency and direction. The shape of these spectra normalized by wave number is given by

.17. $$F(\hat{k})=F(k)k^{5/2}$$

Resio (1987) in a very early attempt to understand the role of wave-wave interactions in shoaling water showed that the observed spectral shape varied as a function of depth and that the remaining energy appeared to be consistent with observed energy variations in spectral shape observed in nature. However, since wave-wave interactions are conservative, there was no source term explicitly contained in that treatment of waves in shoaling water depths, reasonable objections to the inference of related energy losses were noted and were included within the STWAVE (Resio) series of codes.

It is likely that other mechanisms for energy loss in shoaling water have been implemented into most coupled modeling systems of waves and surges; however, as will be shown here, many of the very empirical source terms are likely accounting, at least in part, for the S_{nl} energy-flux losses. For this reason, it is expected that some retuning of appropriate sets of source-term will likely be required. In a physical sense, S_{brk} is the least understood term among the source terms; it is temporally and spatially sporadic and occurs on a much shorter time scale than other major source terms contributing to wave generation and decay (nonlinear resonant interactions and wind input). Hence, despite numerous scientific investigations over the years, S_{brk} has no universally accepted mathematical form (Holthuijsen, 2007). Since the nonlinear fluxes into the k^{-3} region of the spectrum, similar to turbulence in other fluid flows, this “breaking” time scale cascade should be on a much faster time scale than the variation of flux rates due to nonlinear 4-wave interactions. Thus, we assume here that nonlinear interaction fluxes play a minor/negligible role relative the wave breaking past the transition point transition frequency. However, the total energy in the spectrum must consider the additional contributions from the integration over the entire frequency range.

Where Γ_E^+ is the energy flux to higher frequencies by 4-wave interactions, β is the reference wind speed governing momentum transfer into the wave field and λ is a function of the angular distribution of waves contributing to the velocity that causes the wave to break, in this case set to 5. In this paper, we use the constraint that, at the point of transition, the energy densities in the $k^{-5/2}$ range had to transition into a k^{-3} form. Fluxes past this transition would be acc(statistical) energy loss rate due to wave-wave interaction fluxes should be estimated at this matching wavenumber point; and the energy past the this point should b represented with a k^{-3} form, with the coefficient for the energy above that peak given by that coefficient times k^{-3} Wave energy inside this regions should be governed by the conventional ratio of wave heights to depth, which is assumed to be written here as

$$18.\ \mathrm{E}_{0_x} = \left(\varepsilon \hat{d}_x\right)^2$$

where x is the depth as a function of distance along the slope and E_0 is the to energy such that traditional coefficients for the ratio of significant wave height to depth ranges, ε, varies from 1 at the point of transition and ε is the ratio of significant wave height to depth; with dx taken as the distance normal to the shore given a values of 0 at the transition point. Along a normal to the coast pointd_x is the distance from the transition point. To avoid a discontinuity, we let ε is given by $\varepsilon = 1. - .2 d_x$ with a constraint that $\varepsilon = 1. - 0.2 \lambda d_x$, with λ = 0.01 and $\varepsilon \geq 0.8$ is equal. This estimate has only been postulated and not checked for its validity on arbitrary coastal areas and nearshore slopes and requires additional testing. However, this portion of the wave-driven setup is not very dependent on the slope and likely is not the primary term driving set-up or longshore currents.

The wind momentum fluxes into the wave field typically lead to wave growth, however, this source term in typically very small relative to energy losses in the surf zone. In this case, the increasing wavenumbers produce an increased flux to higher wavenumbers and the peak of the spectrum can remain in balance with the shift of the spectral peak into higher wavenumbers. Thus, although wave-wave interactions are conservative, they lead directly to a loss of energy as part of the overall energy balance in waves, similar to the creation of turbulence in atmospheric processes. The reduction in wave energy is well predicted by model such as STWAVE (Resio, 1987, Smith,,….Cialone,) in areas will small slopes but should be modified for conserve energy in a more general sense on steeper slopes, based on the flux rates in equation 3. However in some circumstances, such as locally steep slopes, this equation should be replace by the parameterized flux equation developed here.

Discussion and Conclusions

A kinematic criterion for wave breaking is used here as a limiter for individual wave breaking in a random wave field. It is shown that this form of breaking can be considered within a spectral context using Monte Carlo simulations in which the relevant parameter used to define the breaking limit for transitioning to a breaking dominated form from an equilibrium range form. The point of transition is defined as the frequency at which the ratio of the group velocity associated with that frequency divided by the cumulative horizontal orbital velocity estimated from the sum of orbital velocities produced by lower frequencies exceeds 0.85. It is obvious that all higher frequencies also surpass the limiting value for breaking, so this limit leads to a single breaking event in the wave field. Converting the distribution of breaking events at a given frequency into a cumulative distribution function of frequency allows the estimation of a rate of energy being lost for any particular location of f_{brk}, as explained in section 4.

In this paper, we assume that this breaking rate must match the energy fluxes to high frequency produced by S_{nl}. This hypothesis appears to deviate from the sets of contemporary wave dissipation sink terms used in spectral wind-wave models today. The kinematic breaking criterion used here is supported by several field and lab studies (Saket et al., 2017; Shemer and Liberzon, 2014; Waseda et al., 2014), and is consistent with numerical studies of focused wave phases, for the special case when breaking occurs at the spectral peak (Barthelemy et al., 2018; Derakhti and Kirby, 2016). Essentially all of these papers show a clear association between wave breaking and the ratio of horizontal particle velocities U to the wave group velocity as expected from energy convergence-divergence considerations. In this paper, we generalized this hypothesis to allow spectral breaking in random wave fields with varying sea states to provide a source term consistent with the time and space scale of the other source terms in spectral wave models.

It should be noted that the breaking mechanism is functionally similar to dominant wave breaking, such as investigated by Barthelemy et al., (2018); however, in their work they utilize the convergence of phases in a wave field containing only a small number of wave components, which results in deterministically prescribed energy convergence rates. Their results show that waves break when the combined orbital velocity from all spectral components at the crest exceeds 0.85 times the wave propagation speed, consistent with the ratio used in this paper.

.

The main findings of this work are as follows:

1. Wave fields produced by random-phase simulations show that waves at a range of frequencies above the spectral peak will surpass the kinematic limit for wave breaking at a far greater rate than waves in the vicinity of the spectral peak, consistent with the detailed modeling by Irinonov and Voronovitch (2010) who showed the dominant breaking began at a mid-range of frequencies rather than at the spectral peak or only very high frequencies.
2. An estimate of the transition frequency from a nonlinear energy-flux spectral form (f^{-4}) to a dissipative spectral region (f^{-5}) can be estimated as the point where the mean

rate of breaking (determined by Monte Carlo simulations using the kinematic breaking limit) and the energy contained in the spectral region being dissipated is equal to the nonlinear energy flux through the spectrum directed toward high frequencies.

3. This approximation shows that the transition frequency (f_{brk}) is expected to be proportional to a function of inverse wave age $(C_p/U_{10})^{2/3}$.

4. The relation between the transition frequency derived here is shown to be consistent with observations (Long and Resio, 2007) as shown in table 1. This allows the new breaking term to be adapted for use in operational wave models as a transition frequency predictor.

Acknowledgments

REFERENCES

Alves, J.H.G.M., Banner, M.L., 2003. Performance of a Saturation-Based Dissipation-Rate Source Term in Modeling the Fetch-Limited Evolution of Wind Waves. J. Phys. Oceanogr. 33, 1274–1298. https://doi.org/10.1175/1520-0485(2003)033<1274:POASDS>2.0.CO;2

Ardag, D. and D.T. Resio, 2019. Inconsistent spectral evolution in operational wave models due to inacccurate specification of nonlinear interactions, J.Phys. Oceanogr.49(3),505-722.

Ardag, D. and D.T. Resio,2020. A new approach for modeling dissipation due to breaking in wind wave spectra, J. Phys. Oceangr. 50(2),439-454.

Babanin, A. V., Tsagareli, K.N., Young, I.R., Walker, D.J., 2010. Numerical Investigation of Spectral Evolution of Wind Waves. Part II: Dissipation Term and Evolution Tests. J. Phys. Oceanogr. 40, 667–683. https://doi.org/10.1175/2009JPO4370.1

Babanin, A. V., Young, I.R., Banner, M.L., 2001. Breaking probabilities for dominant surface waves on water of finite constant depth. J. Geophys. Res. 106, 11659. https://doi.org/10.1029/2000JC000215

Banner, M.L., Babanin, A. V., Young, I.R., 2000. Breaking Probability for Dominant Waves on the Sea Surface. J. Phys. Oceanogr. 30, 3145–3160. https://doi.org/10.1175/1520-0485(2000)030<3145:BPFDWO>2.0.CO;2

Banner, M.L., Peirson, W.L., 2007. Wave breaking onset and strength for two-dimensional deep-water wave groups. J. Fluid Mech. 585, 93–115. https://doi.org/10.1017/S0022112007006568

Banner, M.L., Tian, X., 1998. On the determination of the onset of breaking for modulating surface gravity water waves. J. Fluid Mech. 367, S0022112098001517. https://doi.org/10.1017/S0022112098001517

Barthelemy, X., Banner, M.L., Peirson, W.L., Fedele, F., Allis, M., Dias, F., 2018. On a unified breaking onset threshold for gravity waves in deep and intermediate depth water. J. Fluid Mech. 841, 463–488. https://doi.org/10.1017/jfm.2018.93

Birch, K.G., Ewing, J.A., 1986. Observations of Wind Waves on a Reservoir, 234. Institute of Oceanographic Sciences.

.

Donelan, M.A., 1998. Air-water exchange processes, in: Coastal and Estuarine Studies. pp. 19–36. https://doi.org/10.1029/CE054p0019

Duncan, J.H., 1981. An Experimental Investigation of Breaking Waves Produced by a Towed Hydrofoil. Proc. R. Soc. A Math. Phys. Eng. Sci. 377, 331–348. https://doi.org/10.1098/rspa.1981.0127

Forristall, G.Z., 1981. Measurements of a Saturated Range in Ocean Wave Spectra. J. Geophys. Res. Ocean. 86, 8075–8084. https://doi.org/10.1029/JC086iC09p08075

Gerstner, F., 1809. Theorie der Wellen. Ann. Phys. 32, 412–445. https://doi.org/10.1002/andp.18090320808

Hasselmann, K., 1974. On the spectral dissipation of ocean waves due to white capping. Boundary-Layer Meteorol. 6, 107–127. https://doi.org/10.1007/BF00232479

Holthuijsen, L.H., 2007. Waves in Oceanic and Coastal Waters. Oceanography 20, 133–135. https://doi.org/10.5670/oceanog.2007.42

Irisov, V., Voronovich, A., 2011. Numerical Simulation of Wave Breaking. J. Phys. Oceanogr. 41, 346–364. https://doi.org/10.1175/2010JPO4442.1

Komen, G.J., Hasselmann, K., Hasselmann, K., 1984. On the Existence of a Fully Developed Wind-Sea Spectrum. J. Phys. Oceanogr. https://doi.org/10.1175/1520-0485(1984)014<1271:OTEOAF>2.0.CO;2

Lenain, L., Melville, W.K., 2017. Measurements of the directional spectrum across the equilibrium-saturation ranges of wind-generated surface waves. J. Phys. Oceanogr. JPO-D-17-0017.1. https://doi.org/10.1175/JPO-D-17-0017.1

Long, C.E., Resio, D.T., 2007. Wind wave spectral observations in Currituck Sound, North Carolina. J. Geophys. Res. Ocean. 112, C05001. https://doi.org/10.1029/2006JC003835

Melville, W.K., 1996. The Role of Surface-Wave Breaking in Air-Sea Interaction. Annu. Rev. Fluid Mech. 28, 279–321. https://doi.org/10.1146/annurev.fl.28.010196.001431

Onorato, M. , A.R. Osborne and M.Serio (2007). On the relation between two numerical methods for the computation of random gravity waves, Eur.J.Mech. B.Fluids 26,43-48.

Phillips, O.M., 1985. Spectral and statistical properties of the equilibrium range in wind-generated gravity waves. J. Fluid Mech. 156, 505. https://doi.org/10.1017/S0022112085002221

Phillips, O.M., 1958. The equilibrium range in the spectrum of wind-generated waves. J. Fluid Mech. 4, 426–434. https://doi.org/10.1017/S0022112058000550

Rapp, R.J., Melville, W.K., 1990. Laboratory Measurements of Deep-Water Breaking Waves. Philos. Trans. R. Soc. A Math. Phys. Eng. Sci. 331, 735–800. https://doi.org/10.1098/rsta.1990.0098

Resio, D.T.,1987.Shallow water waves I: Theory. J. Waterways, Port, Coast, and Oc Engr, 113 (3) ASCE, 264-281.

Resio D and W. Perrie. 1989.Implications of an f^{-4} equilibrium range for wind generated wave J. Phys., Oceanogr. 19,193-204.

Resio, D.T., Long, C.E., Vincent, L.C., 2004. Equilibrium-range constant in wind-generated wave spectra. J. Geophys. Res. 109, C01018. https://doi.org/10.1029/2003JC001788

Resio, D.T., Pihl, J.H., Tracy, B.A., Vincent, L.C., 2001. Nonlinear energy fluxes and the finite depth equilibrium range in wave spectra. J. Geophys. Res. Ocean. 106, 6985–7000. https://doi.org/10.1029/2000JC900153

Resio, D.T., Long, C.E., Perrie, W., 2011. The Role of Nonlinear Momentum Fluxes on the Evolution of Directional Wind-Wave Spectra. J. Phys. Oceanogr. 41, 781–801. https://doi.org/10.1175/2010JPO4545.1

Resio, D T and D.Ardag. 2016. Chrarcteristics of directional wave spectra and implications for detailed-balance wave modelling,Ocean Modeling 103,38 -52.

Rodríguez, G., Soares, C.G., 1999. Uncertainty in the estimation of the slope of the high frequency tail of wave spectra. Appl. Ocean Res. 21, 207–213. https://doi.org/10.1016/S0141-1187(99)00014-0

Romero, L., Melville, W.K., 2010. Airborne Observations of Fetch-Limited Waves in the Gulf of Tehuantepec. J. Phys. Oceanogr. 40, 441–465. https://doi.org/10.1175/2009JPO4127.1

Romero, L., Melville, W.K., Kleiss, J.M., 2012. Spectral Energy Dissipation due to Surface Wave Breaking. J. Phys. Oceanogr. 42, 1421–1444. https://doi.org/10.1175/JPO-D-11-072.1

Saket, A., Peirson, W.L., Banner, M.L., Barthelemy, X., Allis, M.J., 2017. On the threshold for wave breaking of two-dimensional deep water wave groups in the absence and presence of wind. J. Fluid Mech. 811, 642–658. https://doi.org/10.1017/jfm.2016.776

Schwendeman, M., Thomson, J., Gemmrich, J.R., 2014. Wave Breaking Dissipation in a Young Wind Sea. J. Phys. Oceanogr. 44, 104–127. https://doi.org/10.1175/JPO-D-12-0237.1

Shemer, L., Liberzon, D., 2014. Lagrangian kinematics of steep waves up to the inception of a spilling breaker. Phys. Fluids 26. https://doi.org/10.1063/1.4860235

Smith, J. M. and S. J. Smith. 2002. Grid nesting with STWAVE. ERDC/CHL CHETN I-66. Vicksburg, MS: U.S. Army Engineer Research and Development Center. http://chl.wes.army.lmil/library/publications/chetn/.

Smith, J. M. 2001. Modeling nearshore transformation with STWAVE. ERDC/CHL CHETN I-64. Vicksburg, MS: U.S. Army Engineer Research and Development Center

Song, J.-B., Banner, M.L., 2002. On Determining the Onset and Strength of Breaking for Deep Water Waves. Part I: Unforced Irrotational Wave Groups. J. Phys. Oceanogr. 32, 2541–2558. https://doi.org/10.1175/1520-0485-32.9.2541

Stokes, G.G.S., 1880. Mathematical and physical papers. Cambridge [Eng] : University Press.

Toffoli, A., Babanin, A. V., Onorato, M., Waseda, T., 2010. Maximum steepness of oceanic waves: Field and laboratory. Geophys. Res. Lett. 37, 1–4. https://doi.org/10.1029/2009GL041771

Tulin, M.P., Landrini, M., 2001. Breaking waves in the ocean and around ships, in: Twenty-Second Symposium on Naval Hydrodynamics. National Academies Press, Washington, D.C., pp. 713–745.

Umesh, P.A., Bhaskaran, P.K., Sandhya, K.G., Nair, T.M.B., 2017. High Frequency Tail Characteristics in the Coastal Waters off Gopalpur, Northwest Bay of Bengal: A Nearshore Modelling Study. Pure Appl. Geophys. https://doi.org/10.1007/s00024-017-1761-1

Waseda, T., Sinchi, M., Kiyomatsu, K., Nishida, T., Takahashi, S., Asaumi, S., Kawai, Y., Tamura, H., Miyazawa, Y., 2014. Deep water observations of extreme waves with moored and free GPS buoys. Ocean Dyn. 64, 1269–1280. https://doi.org/10.1007/s10236-014-0751-4

Zakharov, V. E. and N.N.Filonenko, 1967 Weak turbulence of capillary wave, J. Appl Mech and Tech. Phys 8, 37-40

List of Tables

Inverse Wave Age (U/c_p)	Non-Dimensional Transition Frequency (f_{ti})
0.7 and lower	2.9
0.8	2.7
1	2.5
1.2	2.2
1.6	2
2 and higher	1.5

Table 1. Transition frequencies defined by the inverse wave age values.

List of Figures

Figure 1: Compensated and normalized energy densities grouped and averaged according to their inverse wave ages from Long and Resio (2007). Frequencies where the spectral shape transitions to a different form are shown by black dots.

Figure 2: The blue line represents the surface record and the red circles are the zero-upcrossing points defining starting and ending times for each individual wave.

Figure 3: Probability distribution functions for two different simulations under two different conditions, one with a lower wave age (left) and one with a higher wave age. The case for lower wave age breaking probabilities closer to the peak are higher.

Figure 4: f_{brk}/f_p plotted against $(C_p/U_{10})^{2/3}$ to examine the proposed linear form in equation (12) for 6 different wave age values. Blue dots are the mean results for each random set given with error bars (95% confidence limits) (blue line). The linear fit is shown as the red dashed line.

Figure 5: Positive energy fluxes (red line) found by using equation (6) drawn against the breaking energy rate (blue dotted line) for a simulation initiated with a peak frequency of 0.25 Hz and wind speed of 5 m/s. They intersect around 2.5 f/f_p, which denotes the transition frequency under this particular condition.

Figure 6: Normalized transition frequency vs. wave age parameter here are shown for 72 different simulations, each dot represents a simulation. Three different colored lines show linear fits for 0.7, 0.8 and 0.9 breaking rates and the legend shows the R^2 values for each line.

Figure 7: Comparison of f/fb results from unidirectional and directional tests over a range of inverse wave age conditions.

598

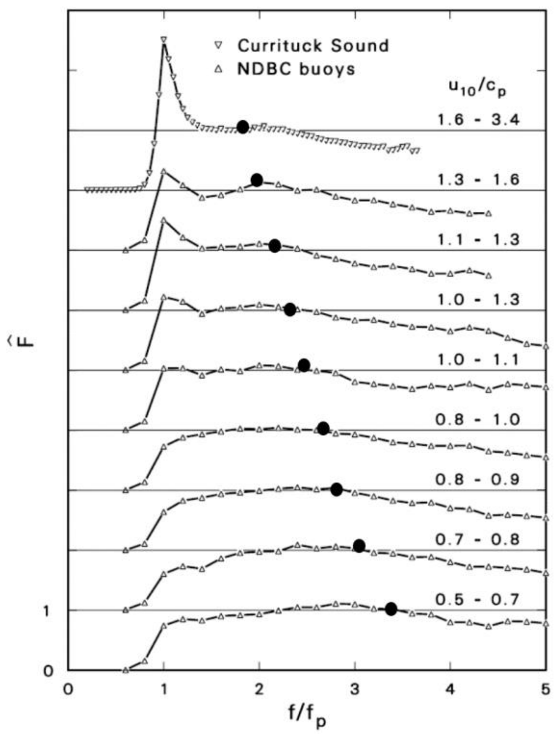

Figure 1. Compensated and normalized spectral energy densities, grouped and averaged according to increments of inverse wave age. The black dots here show that the equilibrium for

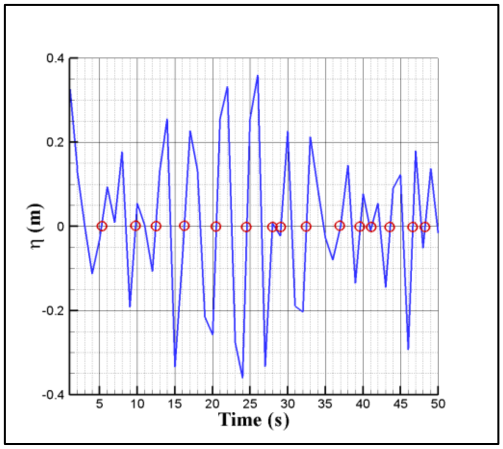

Figure 1~~2~~: The blue line represents the surface record and the red circles are the zero-upcrossing points defining starting and ending times for each individual wave.

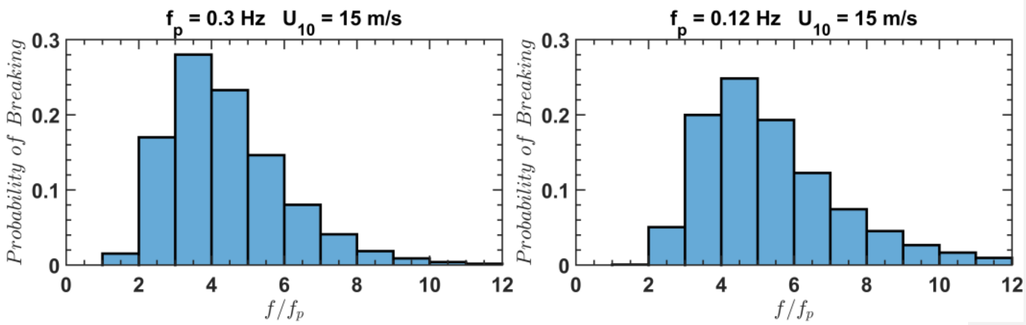

Figure 2~~3~~: Probability distribution functions for two different simulations under two different conditions, one with a lower wave age (left) and one with a higher wave age. The case for lower wave age breaking probabilities closer to the peak are higher.

of the spectra changes shape at some point higher than the spectral peak.

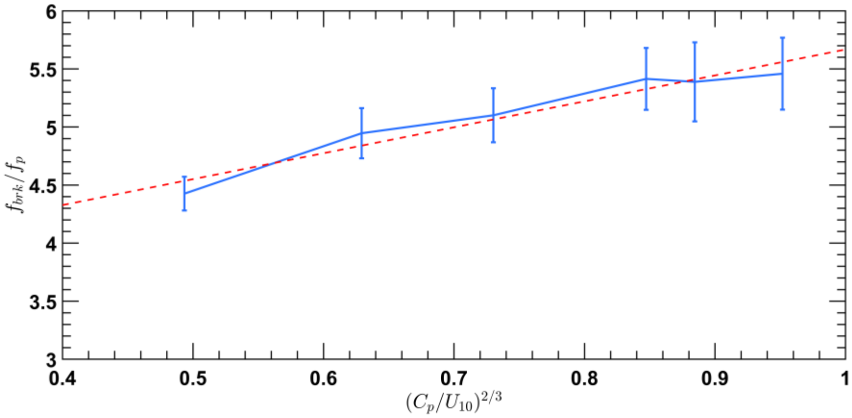

Figure 34: f_{brk}/f_p plotted against $(C_p/U_{10})^{2/3}$ to examine the proposed linear form in equation (12) for 6 different wave age values. Blue dots are the mean results for each random set given with 95% confidence limits (blue line). The linear fit is shown as the red dashed line.

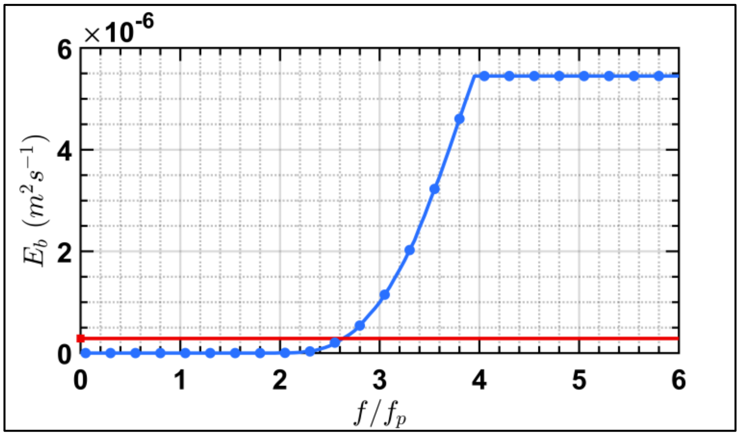

Figure 4~~5~~: Positive energy fluxes (red line) (originated from the peak frequency) found by using equation (6) drawn against the breaking energy rate (blue dotted line) for a simulation initiated with a peak frequency of 0.25 Hz and wind speed of 5 m/s. They intersect around 2.5 f/f_p, which denotes the transition frequency under this particular condition.

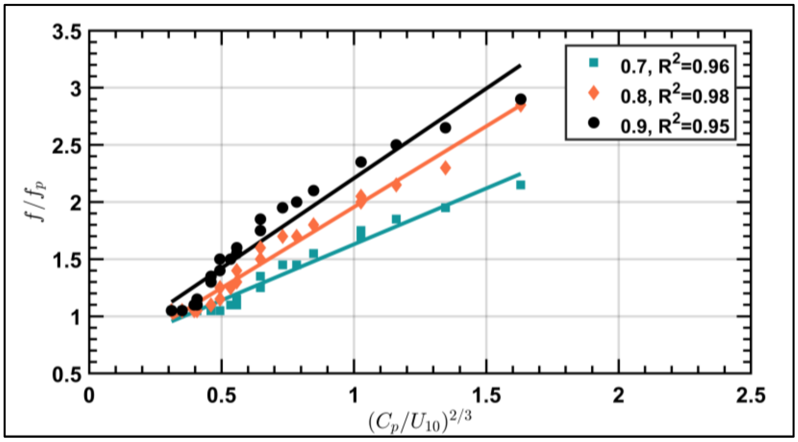

Figure 5~~6~~: Normalized transition frequency vs. wave age parameter here are shown for 72 different simulations, each dot represents a simulation. Three different colored lines show linear fits for 0.7, 0.8 and 0.9 breaking rates and the legend shows the R^2 values for each line.

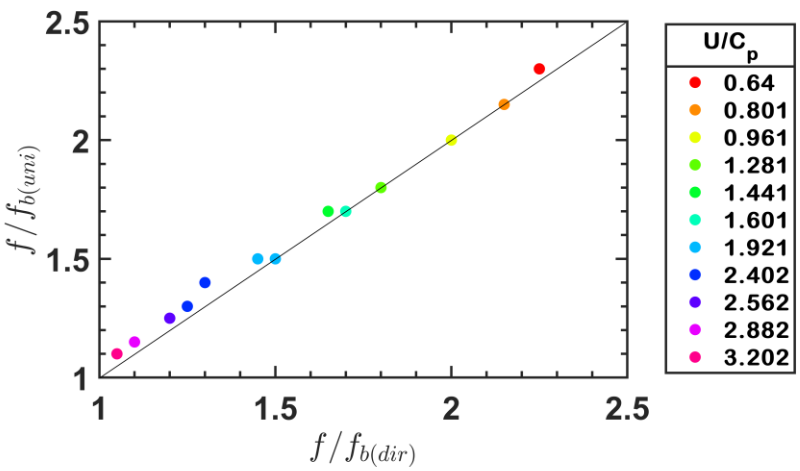

Figure 6~~7~~: Comparison of f/f_b results from unidirectional and directional tests over a range of inverse wave age conditions.